Thermal redistribution and dephasing of localized excitons in CdSe/ZnSSe quantum island structures

H.-P. Tranitz
Institut für Physik, Technische Universität Chemnitz, 09107 Chemnitz, Germany

H. P. Wagner*
Department of Physics, University of Cincinnati, Cincinnati, Ohio 45221-001

R. Engelhardt, U. W. Pohl, and D. Bimberg
Institut für Festkörperphysik, Technische Universität Berlin, 10623 Berlin, Germany
(Received 19 July 2001; published 2 January 2002)

Temperature-dependent photoluminescence measurements of CdSe/ZnSSe quantum island structures show a blueshift of the emission maximum and a significant broadening of the emission band above 50 K. The features originate from a thermal activation of localized excitons and a redistribution of the occupation within the inhomogeneous island ensemble. The presence of exciton states with different localization at comparable transition energies is indicated by a multiexponential decay of the four-wave mixing photon echo observed at low temperatures. Upon increasing the temperature above 50 K, the decay of the four-wave mixing signal changes into a monoexponential behavior. Polarization-dependent measurements unhide strong exciton-exciton interaction and signify the formation of biexcitons with biexciton binding energies around 12 meV. The features indicate the dominance of weakly localized quantum-well-like precursor states of CdSe islands on the high-energy side of the emission band.

DOI: 10.1103/PhysRevB.65.035325 PACS number(s): 78.67.Hc, 42.50.Md, 78.47.+p

I. INTRODUCTION

The persisting interest in II–VI semiconductors is driven by both fundamental aspects concerning, e.g., nonlinear optical properties and the development of new optoelectronic and all-optical devices for the green and blue spectral range. As a mainspring for recent developments emerges the fast progress in growth and characterization of self-organized zero-dimensional structures, i.e., quantum dots or islands,[1,2] leading to improved device features such as reduction of the threshold of lasers[3–6] or efficient waveguiding.[7]

The characterization of the optical properties of quantum dots is dominated by incoherent methods (e.g., Refs. 8 and 9). Recent developments allow investigations with a submicrometer spacial[10–13] or a subnanosecond time[12–15] resolution. Coherent phenomena such as exciton dephasing, the formation of biexcitons, or the exciton-phonon kinetics provide additional information about nature and localization of quantum island states that can be measured using nonlinear four-wave mixing (FWM) spectroscopy.[16–20]

This paper focuses on the thermal activation and dephasing of exciton states in self-organized CdSe/ZnSSe quantum island structures using photoluminescence (PL) and polarization-dependent FWM experiments. The combination of incoherent and coherent methods provide complementary information on differently localized states of CdSe/ZnSSe islands and ZnCdSe well regions. The optical studies reveal a strong contribution of weakly localized states to the PL near the peak maximum that originate from quantum-well-like CdSe quantum island precursors marking the transition from quasi-zero-dimensional quantum island states to quasi-two-dimensional quantum well states.

II. EXPERIMENTAL DETAILS

The quantum island structure studied here was grown by metalorganic vapor phase epitaxy and consists of three CdSe layers with one monolayer nominal thickness, being separated by ZnSSe spacer layers with 5 nm thickness. The CdSe/ZnSSe stack was grown on a (001)-oriented GaAs substrate and a ZnSSe (300 nm) buffer layer, and was sandwiched between two ZnSSe layers (85 nm) and ZnMgSSe barriers (10 nm), finally capped by a ZnSe top layer (5 nm). All layers were grown lattice-matched to the substrate except for the CdSe insertions. As to the insertions, the self-organized growth leads to flat CdSe quantum islands that have a height of 2–3 nm, a lateral width of 2–5 nm, and a density ranging between 3×10^{11} and $1\times10^{12}\,\mathrm{cm}^{-2}$. In lateral extension the islands are embedded in a ZnCdSe quantum well with a locally varying Cd content. Details of the growth process and sample characterization are given in Refs. 21–23.

The FWM experiments were performed in reflection geometry using a two-beam self-diffraction configuration. A frequency-doubled, mode-locked Ti sapphire laser was used as excitation source, producing 100 fs pulses of 22 meV spectral width at a repetition rate of 82 MHz. The focus diameter on the sample was 100 μm at $1/e^2$ intensity. The polarizations of the two incident pulses with directions $\mathbf{k}_1$ and $\mathbf{k}_2$ and a mutual delay time τ were adjusted to co-circular (σ^+,σ^+) as well as linear polarizations with relative angles of 0° ($\uparrow\uparrow$), 45° ($\uparrow\nearrow$), and 90° ($\uparrow\rightarrow$), yielding an excitation power of about 15 MW/cm^2. In the notation given in parentheses the first (second) symbol indicates the polarization of the $\mathbf{k}_1$ ($\mathbf{k}_2$) pulse. The FWM signal was detected time-integrated in the reflected $2\mathbf{k}_2-\mathbf{k}_1$ direction and spectrally

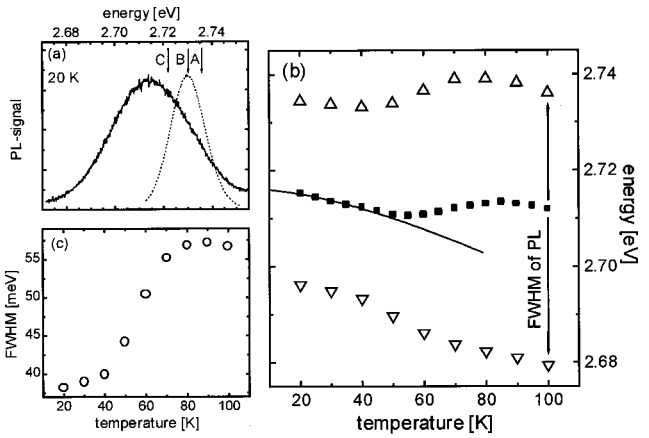

FIG. 1. (a) PL spectrum of the exciton transitions at 20 K. The dashed line shows the spectrum of a 100 fs pulse, the arrows mark the pulse peak energies *A*, *B*, and *C* where FWM experiments were performed. (b) Energy position of the PL band at maximum intensity ($I_{\max}$) (full squares) and the high- (open up-triangle) and low-(open down-triangle) energy value at $I_{\max}/2$ (FWHM) as a function of temperature. The solid line shows a Varshni function according to Eq. (1). (c) FWHM of the PL transition as a function of temperature.

resolved by a combination of a spectrometer and an optical multichannel analyzer. The sample was kept in a helium-flow cryostat for temperature control between 15 and 100 K. The setup was employed also for PL measurements using the Ti:sapphire laser as the excitation source at an excitation energy of about 3 eV.

III. RESULTS AND DISCUSSION

The PL spectrum of the CdSe quantum islands shows a broad band around 2.716 eV with a full width at half maximum (FWHM) $\Delta E \approx 40$ meV at 20 K, arising from the inhomogeneously broadened emission of the island ensemble [Fig. 1(a)]. The dashed line shows the spectral shape of the 100 fs laser pulses used to perform the FWM experiments at the peak positions *A* (2.736 eV), *B* (2.730 eV), and *C* (2.722 eV). The strong blueshift[29] of the PL maximum with respect to the exciton transition in CdSe bulk material at 1.766 eV[24] originates from the quantum confinement and additional effects of strain and island-matrix interdiffusion as discussed in Refs. 25–28. The spectral position of the PL maximum $I_{\max}$ shifts to lower energies when the temperature is raised to 50 K [Fig. 1(b), full squares]. This behavior is well explained by the band-gap reduction at increased temperature. A superimposed effect by phonon-assisted relaxation from less localized exciton states into more localized states[23] is considered to be less important since the redistribution to quantum island states with lower energy leads to a PL band narrowing[29,30,32] that is not observed in the studied sample. Moreover, the observed shift is well described using the Varshni[31] function [solid line in Fig. 1(b)]

$$E(T) = E(0) + \frac{\alpha T^2}{\beta + T}, \tag{1}$$

with parameters $\alpha = 6.96\ \mu$eV/K and $\beta = 281$ K given in Ref. 24 for zinc-blende CdSe and setting $E(0) = 2.7157$ meV. Above 50 K the spectral position of the PL maximum undergoes a blueshift of approximately 3 meV, while above 80 K the maximum emission again starts to shift to lower energies. Such a blueshift in an intermediate temperature range was already previously observed and attributed to a thermally induced redistribution of localized excitons to quantum islands with smaller localization energies or to weakly localized two-dimensional precursor states of the quantum islands[22] within the laterally surrounding ZnCdSe layer. Above 80 K the band-gap reduction overcompensates the energy shift of the PL maximum due to the thermal rearrangement of the excitons, leading to the observed redshift of the exciton emission.

A close look to the change of the FWHM of the PL band with increasing temperature provides a strong indication for the validity of this model. A significant broadening is observed from 38 meV at 20 K to 57 meV at 100 K with a maximum slope between 40 and 80 K [Fig. 1(c)]. The high-(up triangles) and low-(down triangles) energy values at $I_{\max}/2$, i.e., the spectral positions of the FWHM drawn in Fig. 1(b) as a function of temperature demonstrate that the broadening of the PL band mainly occurs on the high energy side. This indicates the redistribution of stronger localized exciton states positioned on the low-energy side to less localized states at the high-energy side leading to the temperature-dependent S-shape evolution of the PL maximum.

To probe the nonlinear and dynamical properties of the CdSe/ZnSSe islands we performed FWM studies using three different spectral positions for the pulse excitation by tuning the central energy to 20 meV (position *A*), 14 meV (position *B*), and 6 meV (position *C*) above the PL maximum position. The FWM signal intensity decreases strongly with decreasing excitation energy, a consequence of the decreasing density of states. Owing to the inhomogeneous broadening of the island emission within the ensemble, a photon echo (PE) is created showing a delayed maximum for $\tau > 0$ and a fast quenching for $\tau < 0$. FWM traces excited at energies *A*, *B*, and *C* and recorded at 15 K on the PE maximum positions are depicted in Fig. 2. The FWM transients show a multiexponential decay indicating differently localized exciton states at comparable transition energies as reported previously for CdSe/ZnSe quantum islands grown by molecular beam epitaxy.[17] The decay of the inhomogeneous distribution of localized excitons is approximately described by a two-exponential function (dashed lines in Fig. 2)

$$I_{\mathrm{FWM}}(\tau > 0) = F e^{-\tau/\tau_f} + S e^{-\tau/\tau_s}, \tag{2}$$

which allows us to extract two components of different dephasing times $T_{2(f/s)} = 4\tau_{(f/s)}$. The fast component *F* is attributed to more delocalized exciton states that show an efficient exciton-exciton scattering and a phonon-assisted relaxation into lower lying states.[17–19] With increasing transition energy (position *C* to *A*), the fraction of these more delocalized exciton states increases, leading to an enhanced dephasing rate as shown in the inset of Fig. 2. The rates correspond to the homogeneous linewidths Γ_f and Γ_s of the

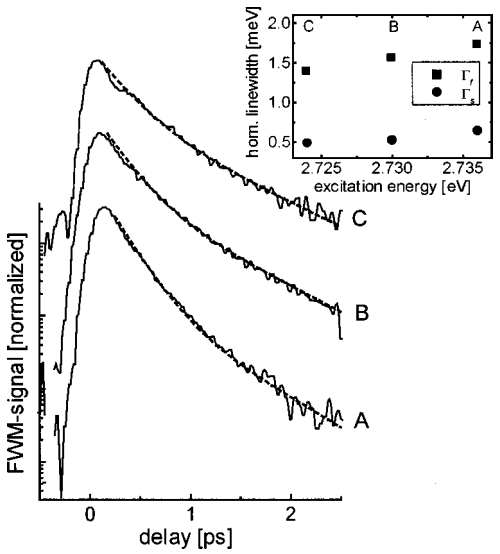

FIG. 2. FWM transients at the excitation energies *A*, *B*, and *C*, recorded at 15 K, dashed lines are two-exponential fits according to Eq. (2). The excitation intensity was 15 MW/cm^2. The inset shows the extracted homogeneous linewidth of the fast and the slow decaying components.

fast and slow decaying component according to the relation $\Gamma_{f/s}=2\hbar/T_{2(f/s)}$. Furthermore, the weight of the fast component *F* with respect to the slow one *S* increases [see Fig. 5(a)]. Accordingly, the slow decaying component *S* is assigned to more localized excitons showing also a slightly increasing dephasing rate with increasing excitation energy.

Further information on the exciton localization is given by polarization-dependent spectrally resolved FWM experiments using cocircular (σ^+,σ^+), colinear $(\uparrow\uparrow)$, $(\uparrow\nearrow)$, and crossed $(\uparrow\rightarrow)$ polarized $\mathbf{k}_1$ and $\mathbf{k}_2$ fields and an analyzer with polarization position *P*. A set of FWM spectra obtained from various configurations $(\mathbf{k}_1,\mathbf{k}_2,P)$ observed at position *C* (2.722 eV) is given in Fig. 3. The spectra were recorded at 20 K and at a positive delay time $\tau=300$ fs for $(\uparrow\nearrow\searrow)$ and $(\uparrow\rightarrow\uparrow)$ polarizations and at $\tau=400$ fs for other configurations. All spectra are normalized with respect to the PE maximum of the $(\uparrow\uparrow\uparrow)$ configuration, and the relative magnification factors of the other PE maxima are given on the right side of each spectrum. With exception of the $(\sigma^+\sigma^+\sigma^+)$ and $(\uparrow\nearrow\rightarrow)$ configurations all FWM spectra show two bands that are separated by an energy $\Delta\approx12$ meV, revealing strongly varying intensity ratios at different polarization configurations. The bands are attributed to transitions of the exciton *X* and the biexciton *XX* within the inhomogeneously broadened ensemble of localized states with $\Delta\approx12$ meV being the biexciton binding energy.

The spectra shown in Fig. 3 can be explained by the polarization dependence of the main generation processes[33] of the FWM signal. In the framework of extended optical Bloch equations (OBE's) the generation is described by phase-space filling (PSF) and by biexciton formation[34–36] (BIF) and excitation-induced dephasing[37,38] (EID); local field effects (LFE's) do not play an important role in II-VI semiconductors.[33] As in quantum wells, the localized exciton *X* eigenstates $|J,J_z\rangle=|1,\pm1\rangle$ are excited by circularly $(\sigma^\pm)$

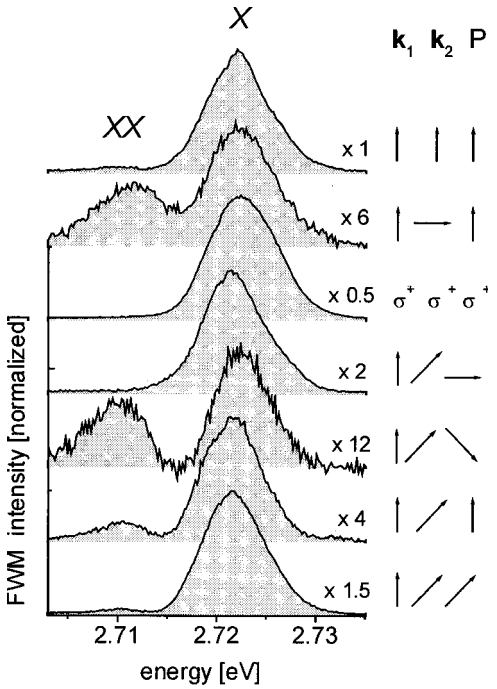

FIG. 3. FWM spectra for different polarization configurations recorded at 20 K and a positive delay time of $\tau=300$ fs for $(\uparrow\nearrow\searrow)$ and $(\uparrow\rightarrow\uparrow)$ polarizations and $\tau=400$ fs for the other configurations. The symbols in the parentheses indicate the polarizations of the excitation pulses propagating along $\mathbf{k}_1$ and $\mathbf{k}_2$ and of the analyzer *P*. The spectra are normalized with respect to the topmost spectrum.

polarized light with dipole matrix vectors $\boldsymbol{\mu}_h^{\pm}=-2^{-0.5}\mu_h(\pm1,i)$ in Jones vector notation. In a homogeneously broadened system the polarization dependence of the third-order polarization $\boldsymbol{P}^{(3)}_{\mathrm{PSF}}$ generated by PSF is given by the solution of the OBE's of a five-level system, in which the calculated Fourier transformed third-order polarization at $\hbar\omega_X$ is proportional to the product of the polarizations of the involved exciton *X* transitions,[39] including also unbound biexciton states.[40,41] The $\boldsymbol{P}^{(3)}_{\mathrm{PSF}}$ generated from the exciton subsystems, e.g., reads

$$\begin{aligned}\boldsymbol{P}^{(3)}_{\mathrm{PSF}}(\hbar\omega_X)\propto&[(\boldsymbol{\mu}^+)^*\cdot\boldsymbol{E}_{\mathbf{k}_2}][(\boldsymbol{\mu}^+)^*\cdot\boldsymbol{E}_{\mathbf{k}_2}][(\boldsymbol{\mu}^+)^*\cdot\boldsymbol{E}_{\mathbf{k}_1}]^*\boldsymbol{\mu}^+\\&+[(\boldsymbol{\mu}^-)^*\cdot\boldsymbol{E}_{\mathbf{k}_2}][(\boldsymbol{\mu}^-)^*\cdot\boldsymbol{E}_{\mathbf{k}_2}]\\&\times[(\boldsymbol{\mu}^-)^*\cdot\boldsymbol{E}_{\mathbf{k}_1}]^*\boldsymbol{\mu}^-.\end{aligned}\tag{3}$$

A detailed analysis of $\boldsymbol{P}^{(3)}_{\mathrm{PSF}}$ including all involved transitions shows that the third-order polarization is $(\uparrow)$ for $(\uparrow\uparrow)$ and $(\uparrow\rightarrow)$ excitation but $(\rightarrow)$ for $(\uparrow\nearrow)$ excitation.

The formation of biexcitons (BIF) is caused by a two-photon excitation. Bound biexcitons *XX* have paired electron as well as hole spins as a consequence of the Pauli exclusion. The *XX* two-photon coherence leading to the BIF FWM is thus created by a simultaneous σ^- and σ^+ excitation by the pulse $\mathbf{k}_2$. The third-order polarization $\boldsymbol{P}^{(3)}_{\mathrm{BIF}}$ is generated by the previously generated $\mathbf{k}_1$ polarization from the two-photon coherence leading to a time-integrated FWM signal $I^{(3)}_{2\mathbf{k}_2-\mathbf{k}_1}(\omega,\tau>0)$ at the *X*-*XX* transition $\hbar\omega_X-\Delta$, where Δ is the

TABLE I. Contribution of phase-space-filling (PSF), biexciton formation (BIF), and excitation-induced dephasing (EID) to the third-order nonlinear polarization $\boldsymbol{P}^{(3)}_{\mathrm{FWM}}$ for different configurations $(\mathbf{k}_1,\mathbf{k}_2,P)$.

Configuration $(\mathbf{k}_1,\mathbf{k}_2,P)$	PSF	BIF	EID
$(\uparrow\uparrow\uparrow)$	1	1	1
$(\uparrow\rightarrow\uparrow)$	1	1	0
$(\sigma^+\sigma^+\sigma^+)$	1	0	1
$(\uparrow\nearrow\rightarrow)$	1	0	1/2
$(\uparrow\nearrow\searrow)$	$1/\sqrt{2}$	$1/\sqrt{2}$	0
$(\uparrow\nearrow\uparrow)$	0	1	1/2
$(\uparrow\nearrow\nearrow)$	$1/\sqrt{2}$	$1/\sqrt{2}$	$1/\sqrt{2}$

biexciton binding energy. The polarization dependence of the *XX* BIF-induced FWM at $\hbar\omega_X-\Delta$ is defined by[39]

$$\boldsymbol{P}^{(3)}_{\mathrm{BIF}}(\hbar\omega_X-\Delta)\propto\sum_{\sigma^+,\sigma^-}\{[(\boldsymbol{\mu}^+)^*\cdot\boldsymbol{E}_{\mathbf{k}_2}][(\boldsymbol{\nu}^-)^*\cdot\boldsymbol{E}_{\mathbf{k}_2}]+[(\boldsymbol{\mu}^-)^*\cdot\boldsymbol{E}_{\mathbf{k}_2}][(\boldsymbol{\nu}^+)^*\cdot\boldsymbol{E}_{\mathbf{k}_2}]\}\times[(\boldsymbol{\mu}^{\pm})^*\cdot\boldsymbol{E}_{\mathbf{k}_1}]^*\boldsymbol{\nu}^{\mp}. \quad (4)$$

The *X* exciton to *XX* biexciton matrix element is given by $\boldsymbol{\nu}^{\pm}$. It vanishes in the (σ^+,σ^+) configuration, since the bound biexciton state *XX* cannot be excited. For linearly polarized excitation fields the direction of the BIF-induced third-order polarization is $(\uparrow)$ for $(\uparrow\uparrow)$, $(\uparrow\rightarrow)$, and $(\uparrow\nearrow)$ excitation, which explains the strong reduction of the *XX* signal in $(\uparrow\nearrow\rightarrow)$ configuration.

In the case of EID the polarization $\boldsymbol{P}^{(3)}_{\mathrm{EID}}$ is caused by a spatially varying exciton-exciton scattering rate within the exciton density grating generated by pulses $\mathbf{k}_1$ and $\mathbf{k}_2$. The resulting spatial modulation of the *X* dephasing time induces a diffraction of pulse $\mathbf{k}_2$ into the direction $2\mathbf{k}_2-\mathbf{k}_1$. Hence the polarization direction of $\boldsymbol{P}^{(3)}_{\mathrm{EID}}$ is the same as that of pulse $\mathbf{k}_2$ and the amplitude of $\boldsymbol{P}^{(3)}_{\mathrm{EID}}$ changes by a factor of $\cos(\theta_{12})$, θ_{12} being the angle between the linear polarization directions of the excitation pulses $\mathbf{k}_1$ and $\mathbf{k}_2$. Consequently the EID component vanishes in $(\uparrow\nearrow\searrow)$ and in $(\uparrow\rightarrow\uparrow)$ configuration. Table I summarizes the contributions of PSF, BIF, and EID to the third-order nonlinear polarization $\boldsymbol{P}^{(3)}_{\mathrm{FWM}}$ at various $(\mathbf{k}_1,\mathbf{k}_2,P)$ configurations obtained from extended OBE's of a homogeneously broadened five-level system.

In addition to the above-mentioned processes disorder induced dephasing (DID) may play an important role in inhomogeneously broadened systems.[42,43] A more detailed analysis of the FWM signal including inhomogeneous broadening and DID will be subject of further investigations.

The FWM measurements indicate that interaction induced processes are dominant in the studied structures, which is unexpected in the case of strongly localized quantum island states where exciton-exciton interaction is anticipated to be significantly reduced. In addition, the signal strength of the *X* band in the $(\uparrow\rightarrow\uparrow)$ configuration is stronger than that of the *XX* band, indicating a clear contribution of biexciton continuum states in this kind of structures. An opposite behavior was previously observed in CdSe/ZnSe quantum islands[17] where a clearly reduced FWM *X* band intensity in $(\uparrow\rightarrow)$ configuration was attributed to a quantization of the biexciton continuum due to island localization. From both observations we follow that the main FWM signal in the CdSe/ZnSSe island structure studied here is generated by weakly localized states. This interpretation is further supported by the low biexciton binding energy $\Delta\approx 12$ meV, which was also extracted from oscillations in the FWM trace[19] that are clearly observable 8 meV below the central excitation energies *A*, *B*, and *C*. The oscillations with a period of $T_p\approx 0.36$ ps originate from the interference between exciton- and biexciton-induced polarizations showing the expected phase shift of π going from the $(\uparrow\uparrow)$ to $(\uparrow\rightarrow)$ configuration.[41] The observed biexciton binding energy is smaller by a factor of 2 than values obtained from CdSe/ZnSe island structures grown by molecular beam epitaxy (MBE) and migration-enhanced epitaxy (MEE)[16–18] at lower temperature. The reduction is attributed to the weaker localization of excitons in this CdSe/ZnSSe sample.

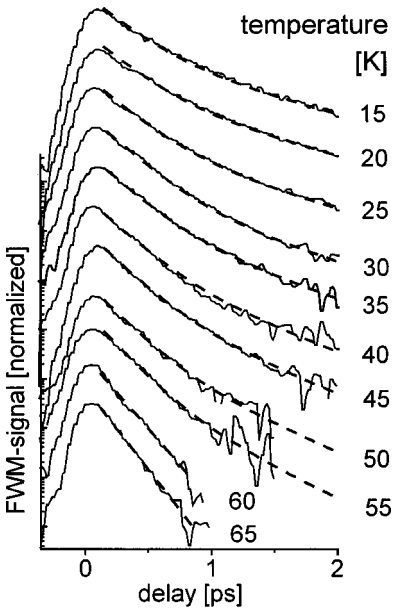

FIG. 4. FWM transients at laser position *B* as a function of temperature. The energy separation between the PL maximum and the excitation position was kept constant over the whole temperature range. The dashed lines show fits using a two-exponential function, Eq. (2), up to 55 K and a monoexponential function above 55 K.

Temperature-dependent FWM measurements that are performed at position *B* provide further information on the exciton localization. The energy separation between the PL maximum and the excitation position was kept constant over the whole temperature range for comparison with low temperature data. Figure 4 shows the normalized FWM traces between 15 and 65 K. The measured PE signal was also described using Eq. (2) up to a temperature of 55 K and a single exponential above 60 K where a distinction of more and less localized exciton states is no longer appropriate.

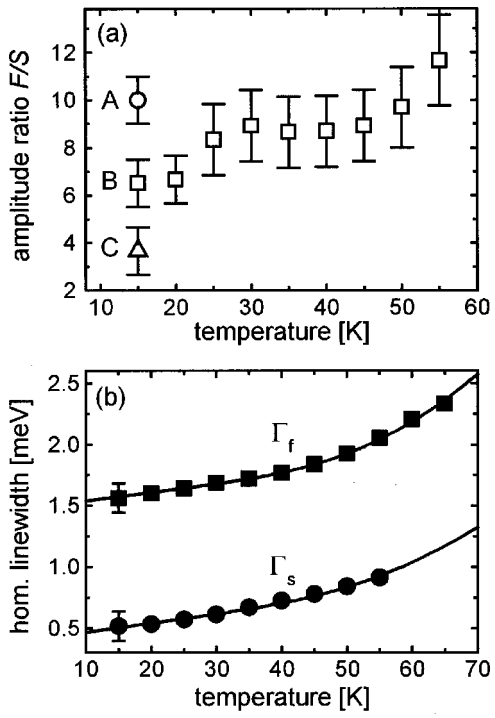

FIG. 5. (a) Amplitude ratio F/S obtained from the two-exponential fit, Eq. (2), as a function of temperature. (b) Homogeneous linewidths $\Gamma_{f/s}$ extracted from the two-exponential and monoexponential fits used in Fig. 4 as a function of temperature; the lines are fits according Eq. (5).

Figure 5(a) shows the amplitude ratio F/S of the fast to slow component extracted from the two-exponential fits as a function of the temperature. A slight increase at the temperatures between 15 and 25 K is attributed to phonon-assisted filling of stronger localized states. Between 25 and 45 K the amplitude ratio remains almost constant, while there is an increase of the ratio above 45 K that is accompanied by the onset of the blueshift of the PL maximum. Above 55 K a slow component is no longer detectable and a monoexponential function fits the experimental data corresponding to the fast decay rate. In addition, we plotted the homogeneous linewidth $\Gamma_{f/s}$ as a function of temperature in Fig. 5(b). The solid lines are fits that describe the increase of the homogeneous linewidth Γ due to exciton-phonon interaction,[44]

$$\Gamma_{f/s}=\Gamma_{f/s}(T=0\ \mathrm{K})+\gamma_{\mathrm{ac}(f/s)}T+\frac{\gamma_{\mathrm{LO}(f/s)}}{e^{(E_{\mathrm{LO}}/k_BT)}-1}. \qquad (5)$$

γ_{ac} and γ_{LO} denote the phonon scattering parameters and k_B is the Boltzmann constant. Using a LO-phonon energy $E_{\mathrm{LO}}=26$ meV of CdSe,[20] the homogeneous linewidth at zero lattice temperature $\Gamma_{f/s}(T=0)$ are found to be 1.47 meV for the fast and 0.39 meV for the slow component. These linewidths exceed the FWHM of single island emission lines obtained by cathodoluminescence[23] by more than one order of magnitude. The variance is explained by the strong density-dependent exciton-exciton scattering processes (EID) since high pulse powers are used in FWM. The exciton–acoustic-phonon scattering parameters $\gamma_{\mathrm{ac}(f/s)}$ for the fast and slow components are determined to 7 ± 1 and 7.5 ± 1 μeV/K, respectively, and the exciton–LO-phonon scattering parameter $\gamma_{\mathrm{LO}(f)}$ is extracted to be 45 ± 5 meV. Both scattering parameters are close to values reported from ZnCdSe/ZnSe quantum wells,[45,46] thus indicating that exciton-phonon interaction is not significantly modified in these islands but would be expected in the case of strong three-dimensional confinement.[47,48]

The comparable exciton–acoustic-phonon scattering parameters $\gamma_{\mathrm{ac}(f/s)}$ further indicate that the localization potential even for the more localized states is only a few meV, indicating the dominance of weak localization potentials in the sample. The missing narrowing of the PL band and the observed band broadening between 15 and 50 K further indicate that the weak exciton localization on the high-energy side of the PL band is induced by fluctuations within the two-dimensional precursor states of the quantum islands during the formation process as reported recently for ZnSe-capped CdSe islands.[32]

IV. CONCLUSION

Thermal activation and dephasing of excitons are studied in a self-organized multiple stacked CdSe/ZnSSe quantum island structure grown by metal organic vapor phase epitaxy (MOVPE), using temperature-dependent PL and spectrally resolved FWM. The PL maximum shows an anomalous blueshift and a large broadening of the PL band between 50 and 80 K, which is assigned to a thermal activation of more localized to less localized excitons in quantum islands and to more delocalized states corresponding to quantum-well-like precursors of the CdSe islands. Polarization-dependent FWM experiments on the high-energy side of the PL band indicate that the photon echo is mainly generated by weakly localized excitons that show a strong interaction-induced dephasing and contributions of biexciton continuum states. A biexciton binding energy of 12 meV is found from spectrally resolved FWM and the photon echo oscillation period, smaller than a factor of 2 compared to island structures grown by MBE. The redistribution of localized excitons is further indicated by temperature-dependent FWM measurements that show a multiexponential dephasing at temperatures below 55 K evolving to a monoexponential decay above. From the optical studies we conclude that the excitonic emission of the quantum island structure grown by MOVPE is strongly influenced by precursor states of the CdSe quantum islands that provide only weak localization.

ACKNOWLEDGMENT

The experimental support of H. Schmitzer, A. Pistelok, and R. Schuster is kindly acknowledged. This work was supported by the Deutsche Forschungsgemeinschaft, projects Wa788/3 and SFB296/A7.

*Email address: hp.wagner@physik.tu-chemnitz.de

[1] Y. Arakawa and A. Yariv, IEEE J. Quantum Electron. **22**, 1887 (1986).
[2] D. Bimberg, M. Grundmann, and N. N. Ledentsov, *Quantum Dot Heterosructures* (Wiley, Chichester, 1999).
[3] P. G. Eliseev, H. Li, A. Stintz, G. T. Liu, T. C. Newell, K. J. Malloy, and L. F. Lester, Appl. Phys. Lett. **77**, 262 (2000).
[4] C. W. Snyder, B. G. Orr, D. Kessler, and L. M. Sander, Phys. Rev. Lett. **66**, 3032 (1991).
[5] N. N. Ledentsov, I. L. Krestinov, M. V. Maximov, S. L. Sorokin, P. S. Kop'ev, Zh. I. Alferov, D. Bimberg, and C. M. S. Torres, Appl. Phys. Lett. **69**, 1343 (1996).
[6] S. V. Ivanov, A. A. Toropov, S. V. Sorokin, I. V. Sedova, H. J. Lugauer, G. Reuscher, M. Keim, F. Fischer, A. Waag, and G. Landwehr, Appl. Phys. Lett. **74**, 498 (1999).
[7] M. Strassburg, V. Kator, U. W. Pohl, A. Hoffmann, J. Broser, N. N. Ledentsov, D. Bimberg, A. Rosenauer, U. Fischer, D. Gerthsen, I. L. Krestnikov, M. V. Maximov, P. S. Kop'ev, and Zh. I. Alferov, Appl. Phys. Lett. **72**, 942 (1998).
[8] M. Grundmann, J. Christen, N. N. Ledentsov, J. Böhrer, D. Bimberg, S. S. Ruvimov, P. Werner, U. Richter, U. Gösele, J. Heydenreich, V. M. Ustimov, A. Yu. Egorov, A. E. Zhukov, P. S. Kop'ev, and Zh. I. Alferov, Phys. Rev. Lett. **74**, 4043 (1995).
[9] J. A. Prietro, G. Armelles, T. Vtzmeier, F. Briones, J. C. Ferrer, F. Peiro, A. Cornet, and J. R. Morante, Phys. Rev. Lett. **80**, 1094 (1998).
[10] M. Grün, F. Funfrock, P. Schunk, Th. Schimmel, M. Hetterich, and C. Klingshirn, Appl. Phys. Lett. **73**, 1343 (1998).
[11] M. Lowisch, M. Rabe, F. Kreller, and F. Henneberger, Appl. Phys. Lett. **74**, 2489 (1999).
[12] L. M. Robinson, H. Rho, J. C. Kim, H. E. Jackson, L. M. Smith, S. Lee, M. Dobrowolska, and J. K. Furdyna, Phys. Rev. Lett. **83**, 2797 (1999).
[13] V. Türck, S. Rodt, R. Heitz, O. Stier, M. Strassburg, U. W. Pohl, and D. Bimberg, Phys. Status Solidi B **224**, 217 (2001).
[14] S. V. Ivanov, A. A. Toropov, T. V. Shubina, A. V. Lebedev, I. V. Sedova, P. S. Kop'ev, G. R. Pozina, J. P. Bergmann, and B. Monemar, J. Appl. Phys. **83**, 3186 (1998).
[15] B. P. Zhang, K. Wakatsuki, D. D. Manh, and Y. Segawa, J. Appl. Phys. **88**, 4916 (2000).
[16] F. Gindele, U. Woggon, W. Langbein, J. M. Hvam, K. Leonardi, D. Hommel, and H. Selke, Phys. Rev. B **60**, 8773 (1999).
[17] H. P. Wagner, H.-P. Tranitz, H. Preis, W. Langbein, K. Leosson, and J. M. Hvam, Phys. Rev. B **60**, 10 640 (1999).
[18] H. P. Wagner, H.-P. Tranitz, H. Preis, W. Langbein, and J. M. Hvam, J. Cryst. Growth **214/215**, 747 (2000).
[19] H. P. Wagner, H.-P. Tranitz, R. Schuster, R. Engelhardt, U. W. Pohl, D. Bimberg, Phys. Status Solidi B **224**, 195 (2001).
[20] U. Woggon, F. Gindele, W. Langbein, and J. M. Hvam, Phys. Rev. B **61**, 1935 (2000).
[21] U. W. Pohl, R. Engelhardt, V. Türck, and D. Bimberg, J. Cryst. Growth **195**, 569 (1998).
[22] R. Engelhardt, U. W. Pohl, D. Bimberg, D. Litvinov, A. Rosenauer, and D. Gerthsen, J. Appl. Phys. **86**, 5578 (1999).
[23] V. Türck, S. Rodt, O. Stier, R. Heitz, U. W. Pohl, R. Engelhardt, D. Bimberg, and R. Steingrüber, Phys. Rev. B **61**, 9944 (2000).
[24] W. Shan, J. J. Song, H. Luo, and J. K. Furdyna, Phys. Rev. B **50**, 8012 (1994).
[25] S. Fujita, Y. Wu, Y. Kawakami, and S. Fujita, J. Appl. Phys. **72**, 5233 (1992).
[26] F. Flack and N. Samarth, V. Nikitin, P. A. Crowell, J. Shi, J. Levi, and D. D. Awschalom, Phys. Rev. B **54**, R17 312 (1996).
[27] K. Leonardi, H. Heinke, K. Ohkawa, and D. Hommel, Appl. Phys. Lett. **71**, 1510 (1997).
[28] F. Gindele, C. Märkle, U. Woggon, W. Langbein, J. M. Hvam, K. Leonardi, K. Okawa, and D. Hommel, J. Cryst. Growth **184/185**, 306 (1998).
[29] D. I. Lubyshev, P. P. Gonzáles-Borrero, E. Marega, Jr., E. Petitprez, N. La Scala, Jr., and P. Basmaji, Appl. Phys. Lett. **68**, 205 (1996).
[30] Z. Y. Xu, Z. D. Lu, X. P. Yang, Z. L. Yuan, B. Z. Zheng, and J. Z. Xu, W. K. Ge, Y. Wang, J. Wang, and L. L. Chang, Phys. Rev. B **54**, 11 528 (1996).
[31] Y. P. Varshni, Physica (Utrecht) **34**, 149 (1967).
[32] C. S. Kim, M. Kim, J. K. Furdyna, M. Dobrowolska, S. Lee, H. Rho, L. M. Smith, Howard E. Jackson, E. M. James, Y. Xin, and N. D. Browning, Phys. Rev. Lett. **85**, 1124 (2000).
[33] H. P. Wagner, A. Schätz, W. Langbein, J. M. Hvam, and A. L. Smirl, Phys. Rev. B **60**, 4454 (1999).
[34] K. Bott, O. Heller, D. Bennhardt, S. T. Cundiff, P. Thomas, E. J. Mayer, G. O. Smith, R. Eccleston, J. Kuhl, and K. Ploog, Phys. Rev. B **48**, 17 418 (1993).
[35] H. Wang, J. Shah, T. C. Damen, and L. N. Pfeiffer, Solid State Commun. **91**, 869 (1994).
[36] Y. Z. Hu, R. Binder, S. W. Koch, S. T. Cundiff, H. Wang, and D. G. Steel, Phys. Rev. B **49**, 14 382 (1994).
[37] H. Wang, K. Ferrio, D. G. Steel, Y. Z. Hu, R. Binder, and S. W. Koch, Phys. Rev. Lett. **71**, 1261 (1993).
[38] H. Wang, K. B. Ferrio, D. G. Steel, P. R. Berman, Y. Z. Hu, R. Binder, and S. W. Koch, Phys. Rev. A **49**, R1551 (1994).
[39] K. Bott, E. J. Mayer, G. O. Smith, V. Heuckeroth, M. Hübner, J. Kuhl, T. Meier, A. Schulze, M. Lindberg, S. W. Koch, P. Thomas, R. Hey, and K. Ploog, J. Opt. Soc. Am. B **13**, 1026 (1996).
[40] A. E. Paul, J. A. Bolger, A. L. Smirl, and J. G. Pelegrino, J. Opt. Soc. Am. B **13**, 1016 (1996).
[41] T. F. Albrecht, K. Bott, T. Meier, M. Koch, S. T. Cundiff, J. Feldmann, W. Stolz, P. Thomas, S. W. Koch, and E. O. Göbel, Phys. Rev. B **54**, 4436 (1996).
[42] D. Bennhardt, P. Thomas, R. Eccleston, E . J. Mayer, and J. Kuhl, Phys. Rev. B **47**, 13 485 (1993).
[43] S. Weiser, T. Meier, T. Möbius, A. Euteneuer, E. J. Mayer, W. Stolz, M. Hoffmann, W. W. Rühle, P. Thomas, and S. W. Koch, Phys. Rev. B **63**, 13 088 (2000).
[44] S. Rudin, T. L. Reinecke, and B. Segall, Phys. Rev. B **42**, 11 218 (1990).
[45] A. J. Fischer, D. S. Kim, J. Hays, W. Shan, J. J. Song, D. B. Eason, J. Ren, J. F. Schetzina, H. Luo, J. K. Furdyna, Z. Q. Zhu, T. Yao, J. F. Kiem, and W. Schäfer, Phys. Rev. Lett. **73**, 2368 (1994).
[46] N. T. Pelekanos, J. Ding, M. Hagerott, A. V. Nurmikko, H. Luo, N. Samarth, and J. K. Furdyna, Phys. Rev. B **45**, 6037 (1992).
[47] T. Takagahara, Phys. Rev. B **60**, 2638 (1999).
[48] F. Gindele, K. Hild, W. Langbein, and U. Woggon, Phys. Rev. B **60**, R2157 (1999).